

The remote effect of the Tibetan Plateau on downstream flow in early summer

Yafei Wang,¹ Xiangde Xu,¹ Anthony R. Lupo,² Pingyun Li,³ and Zhicong Yin⁴

Received 20 March 2011; revised 25 July 2011; accepted 26 July 2011; published 11 October 2011.

[1] By using numerical experiments and observational data, this study examined the uplifting and thermal effects of the Tibetan Plateau (TP) on downstream airflow in early summer. Our principal finding is that the uplifting effect of the TP in an Atmospheric General Climate Model (AGCM), including air made warmer than its surroundings climatologically by the huge topography, results mainly in a local response in the atmosphere, i.e., a large ridge north of the TP in the troposphere in June. There was no Rossby wave response to the uplifting effect. However, simulations and statistical analyses strongly suggested that the anomalous TP atmospheric heating associated with global climate warming tends to excite a Rossby wave originating from the TP via Lake Baikal and continuing to move through the Okhotsk Sea to downstream areas. The appearance of the Rossby wave coincides with the positive phase of the eastern part of a normal stationary wave originating in the Caspian Sea traveling via the Okhotsk Sea to the sea area east of Japan that often occurs in June. Thus the TP atmospheric heating acts as an additional wave source in relaying and enhancing the eastern part of the normal wave propagation. Its path usually lies beyond 40°N latitude, which is where the westerly jet stream takes over the role of waveguide.

Citation: Wang, Y., X. Xu, A. R. Lupo, P. Li, and Z. Yin (2011), The remote effect of the Tibetan Plateau on downstream flow in early summer, *J. Geophys. Res.*, 116, D19108, doi:10.1029/2011JD015979.

1. Introduction

[2] The Tibetan Plateau (TP), often referred to as the roof of the world, plays multiple roles in climate variability. The TP influences on weather can be described simply as caused by its vast topography and warm air sources. The massive topography of the TP plays a role in changes of the wind direction when the midlatitude westerlies pass over it [e.g., Manabe and Terpstra, 1974, Murakami, 1981]. A strong, split airflow effect may result in a ridge to the north and a trough to the south of the TP at most levels in the troposphere. A simulation indicated that the current Asian monsoon could not be reproduced without the existence of the TP [Hahn and Manabe, 1975]. As for the lower troposphere, a widespread stationary low pressure area is formed around the TP including South Asia nearly simultaneously with the onset of the global-scale Asian summer monsoon, resulting in the strong low-level southerlies that invade East Asia [Kato, 1989]. However, the heat low is associated with

the latent heat release by the monsoon rain together with the heating from the ground over the TP.

[3] On the other hand, the Himalayan torque that is related mainly to the height of the TP, and the difference in surface pressure between the eastern and western TP environment, are important factors in the variation of atmospheric angular momentum (AAM). The mechanical effect of the TP or the Himalayan torque can play a role in forcing various atmospheric phenomena. The torque is responsible for much of the high-frequency fluctuations in AAM [Iskenderian and Salstein, 1998; Weickmann, 2003]. Further, AAM activity is associated with low frequency oscillations such as the Arctic oscillation and the Pacific North American Pattern, as shown by Lott *et al.* [2001].

[4] Thermal forcing naturally occurs over high land because short wave solar radiation can directly heat the soil surface as it passes through the atmosphere; this causes a linear decrease in air temperature with an increase in the height of the troposphere over a local land. Thus, the warmer air over the TP naturally acts as an elevated heat island in the surrounding atmosphere. A strong heat island in the middle troposphere accompanied by strong convective activity results in both local and remote atmospheric circulation changes [e.g., Ye and Wu, 1998], and this idea is similar to that of convection generated near the surface [e.g., Hoskins and Karoly, 1981; Renwick and Revell, 1999]. In addition, global climate warming strengthens this heat island effect. Wang *et al.* [2008] pointed out that the summer surface air temperature over the TP has increased about 2 K since the 1950s. Their research explored the relationship

¹State Key Laboratory of Severe Weather Chinese Academy of Meteorological Sciences, Beijing, China.

²Department of Soil, Environmental, and Atmospheric Sciences, University of Missouri, Columbia, Missouri, USA.

³Shanxi Meteorological Observatory, Shanxi Meteorological Bureau, Xian, China.

⁴Beijing Meteorological Bureau, Beijing, China.

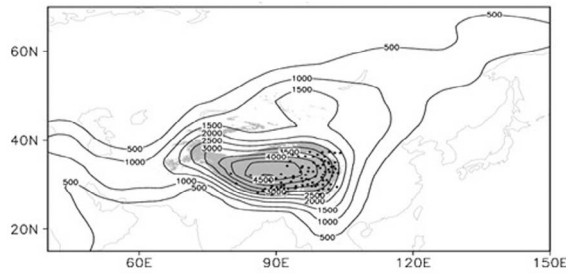


Figure 1. The topographic height with 500 m interval in CAM 3.1 (contour lines) and the locations for surface air temperature (full cycles). The shaded area indicates the Tibetan Plateau regions produced using map board, and the Okhotsk Sea is edged with the coastline in the upper right corner of the map.

between the TP and global warming, and the effect of the TP on atmospheric circulation. The fact that the pace of warming attributed to the anomalous heating source over the TP is accelerating much more rapidly than that of the warming over the rest of the globe (about 0.6°C rising in 20th century [see *Intergovernmental Panel on Climate Change (IPCC)*, 2007]) is likely to result in greater attention to the former.

[5] Numerous studies have pointed out that the TP plays a role in exciting Rossby waves. For example, some simulations showed that the TP thermal effect could cause a series of wave trains to originate from the TP along the jet stream at about 40°N in summer [Wang *et al.*, 2008; Liu *et al.*, 2007; Sato and Kimura, 2007]. The results of these simulations support the waveguide theory proposed by Hoskins and Ambrizzi [1993], who demonstrated that Rossby waves with zonal wave number 7 tend to be trapped by the jet stream from North Africa to the western North Pacific. However, these wave patterns actually occur less frequently than in the model simulations, especially in early summer due to their limited decorrelation time scales. Instead, another kind of wave, called the Okhotsk-Japan (OKJ) pattern, which originates in the Caspian Sea and travels via the Okhotsk Sea to Pacific Ocean east of Japan, is much more active in June [Wang, 1992; Wang and Yasunari, 1994; Nakamura and Fukamachi, 2004; Wang *et al.*, 2007]. East Asian weather is influenced mainly by the OKJ propagation in early summer, because the eastern portion of the wave train disperses with larger amplitude than the western part. Ogi *et al.* [2004] and Wang *et al.* [2007] pointed out that there may be multiple wave sources for the OKJ propagation, although the major one is located around the Caspian Sea. Note that the stronger part of the OKJ is positioned just downstream from the TP. Although Wang *et al.* [2008] provided a reasonable explanation for the impact of TP warming on the general circulation in East Asian summer, the impact may still be different in each summer month. For example, circulation patterns tend to occur differently during June, July, and August, respectively, as noted by Wang [1992] and Sato and Takahashi [2006, 2007]. The OKJ Rossby propagation tends to occur in early summer in particular, while another Rossby-type propagation (P-J) that usually originates from

the Philippines region and continues northwestward into North America appears more frequently in late summer [Wang *et al.*, 2007]. Thus the question is whether the OKJ propagation is partly affected by the TP influence in early summer. This study examines the remote influence of the giant topography, and especially atmospheric heating of the TP on the OKJ propagation in early summer.

[6] In section 2, the data and relevant details of the models are provided. A statistical analysis of the TP heating is carried out in section 3. In sections 4 and 5, an examination of the TP effects is conducted using both longer time integration in an Atmospheric General Circulation Model (AGCM) and a shorter time integration in a regional climate model, respectively. In both models, diabatic sources of TP heating were imposed. Additionally, simulations were run in section 5 in order to test several increased heating scenarios that may accompany climate warming. Such experiments using the techniques discussed in this work are new and, to the authors' knowledge, do not appear elsewhere in the literature. Although the mechanical effect was not the focal point of this work, the related topic (i.e., uplifting effect of the TP) was analyzed in section 4 in order to confirm the integrity of the study of the all TP effects. Finally, section 6 provides a discussion that highlights the main results.

2. Data and Methods

2.1. Data

[7] The National Centers for Environmental Prediction/National Center for Atmospheric Research global atmospheric reanalysis data set was the primary data set used in this study. A detailed description of the data assimilation system that produced this data set was given by Kalnay *et al.* [1996]. In order to calculate the heat source, we used the daily surface sensible heat net flux and precipitation rate from 1 January to 31 December for the years 1960–2007, and the monthly surface net shortwave radiation flux, surface net longwave radiation flux, downward/upward solar radiation flux at tropopause, outgoing longwave radiation at the tropopause, skin temperature and air temperature at 2 m in a T62 Gaussian grid with 192×94 points in June for the years 1960–2007. Appendix A describes the calculation of the heat source in detail. The monthly geopotential height at 500 hPa (Z500), the monthly zonal wind at 500 hPa (U500), and the monthly air temperature for the 90 stations located in the TP in June for the years 1960–2007 were used. The Z500 and U500 have a horizontal resolution of 2.5° latitude-longitude grid. The locations of the stations for air temperature are plotted in Figure 1. Note that the elements we adopted have more robust diurnal variation in the TP than for other regions (not shown), but this variation has been reduced when averaged temporally.

2.2. Models and Experimental Setups

2.2.1. Experiments in Climatic Integration

[8] We used the Community Atmosphere Model 3.1 (CAM3.1) here, which is a widely used, publicly available AGCM that serves as the atmospheric component of the Community Climate System Model Version 3.0. The model has 26 vertical levels and a horizontal spectral resolution of T42, approximately 2.8° latitude by 2.8° longitude when transformed to a Gaussian grid. The model has its own

Table 1. The RegCM3.1 Configuration

Model Component	Description
Grid system	Horizontal: 120×88 grid with about 90 km resolution centered at (45°N , 120°E) Buffer zone: 18 Grids, with an exponential relaxation technique Vertical: 18 layers with sigma coordinate, top pressure is 50 hPa
Physics	Surface physics: BATS; planetary boundary layer scheme: Holtslag, radiation scheme of the NCAR CCM3; Convective Precipitation Schemes: Grell
Artificial heat source	A heat source over the TP ($27.5\text{--}37.5^\circ\text{N}$, $75\text{--}104^\circ\text{E}$) with an maximum heating rate in the boundary layer being from 2 K/day to 8 K/day, and above the boundary with an e-folding height of about 2.5 km
Boundary	The data averaged for June from 1979 to 2001, which was adopted by 40-yr Medium-Range Weather Forecasts reanalysis data set
SST	The data averaged for June from 1979 to 2001, which was adopted by global ocean surface temperature (GISST) data set
Duration	1–30 June

initial data that starts the time integration consistent with spectral truncation. We adopted the Data Ocean Model, which drives the model atmosphere by taking monthly mean sea surface temperature (SST) as a boundary field for our experiments. The SST and sea ice concentrations are used in stand-alone integrations of the CAM3.1. These data sets prescribe analyzed monthly midpoint mean values of SST and ice concentration for the period 1950 through 2001. The data sets are blended products that combine the global Hadley Centre Sea Ice and Sea Surface Temperature data set [Rayner *et al.* 2003] for years up to 1981 and the Reynolds *et al.* [2002] data set after 1981. A community land model 3.0 (CLM3.0) that tasks the impacts of terrestrial ecosystems on climate was coupled to the CAM3.1. More details are available in the model documentation [Collins *et al.* 2004]. The experiments examined two different forcing aspects: (1) uplifting forcing by cutting off the TP with CAM3.1, and (2) thermal forcing by setting up a diabatic heat source on the TP with coupled CAM3.1 and CLM3.0. Note that the uplifting forcing included the heat source naturally existing in elevated topography here. For the brevity, we call such a forcing (effect) the uplifting forcing (effect) to distinguish from the thermal forcing (effect) by adding diabatic heating into the atmosphere in this article. This one approximates the recognized mechanical forcing.

[9] In experiment 1, a control run (UP-Ctr. run) was produced using a 50-year integration with the original model initial condition data set. Figure 1 shows the TP topography height contour line in the model. Note that the 500 m contour line extends as far as the vicinity of the Okhotsk Sea. Thus the height below 1000 m can be regarded as the natural topography that extends over a wide region of East Asia. Retaining the model topography below 1000 m is useful in representing the original climatic conditions that exist in Eurasia outside the area of the TP.

[10] A sensitivity test (UP-ST run) was done in the same manner as the UP-Ctr. run, except for reducing the topography of the TP to 1000 m. The difference between the two integrations in the last 30 years was used to calculate the uplifting effect of the TP. In experiment 2, the two sensitivity tests were integrated for 10 years. Based on the experiment of Wang *et al.* [2008], the two tests were designed to decrease and increase the land surface albedo in the TP area of ($27.5\text{--}37.5^\circ\text{N}$, $75\text{--}105^\circ\text{E}$) for a warm run (H-W run) and a cooling run (H-C run), respectively. We reduced and increased surface albedo to 95 and 105%, respectively, of its current value to cause the surface warming

and cooling for the TP correspondingly. For simplicity, the role of the canopy radiative transfer was not examined. This experiment was designed to obtain the warming and cooling effects of the TP as was similarly done by Wang *et al.* [2008]. More details related with analysis can be found in section 4.

2.2.2. Experiments in Synoptic Integration

[11] A high-resolution Regional Climate Model (RegCM3.1) that was developed by the International Center for Theoretical Physics was used to further investigate the thermal effect of the TP in a synoptic time scale. A detailed description of the three-dimensional, sigma-coordinate, primitive equation regional climate model may be found at <http://users.ictp.it/RegCNET/model.html#description>. The climatological June mean was derived as the model basic state (ReB). The TP warming was simulated by imposing a thermal source with the heating rate 2 K day^{-1} to 8 K day^{-1} with the 2 K's interval on the boundary layer of the TP area (hereafter referred to as H-Re2, H-Re4, H-Re6, and H-Re8), respectively. The heating rate decreased with height exponentially with an e-folding height to the 2.5 km height from the surface, a similar strategy to that used by others [e.g., Tilly *et al.*, 2008]. The model configuration is summarized in Table 1.

3. Statistical Analysis for the TP Heating

[12] The thermal effect represented by the anomalous heating for the TP can be significant in changing atmospheric circulation. Surface air temperature and a column heat source were chosen for the measurement of anomalous heating over the TP. The diabatic column heat source adopted from the Q1 of Yanai *et al.* [1992] was an apparent heating rate that was vertically integrated from the surface to the top of the troposphere. More details about the column heat source are provided in Appendix A. Note that the surface air temperature as a measure of thermal forcing may positively affect the column heat source. However, the surface air temperature results directly from a solar heating and is dependent on the states of land surface and sky over the TP. On the other hand, the net effect of the column heat source depends in part on the advection of heating from other places into the TP region as a result of the heating in the whole troposphere. The surface air temperature as a measure of thermal forcing may be associated more directly with global warming. The surface heating, whether just above the surface or extending into the whole troposphere, is a major factor that generates downstream Rossby wave propagation [e.g., Hoskins and Karoly, 1981; Renwick and Revell, 1999].

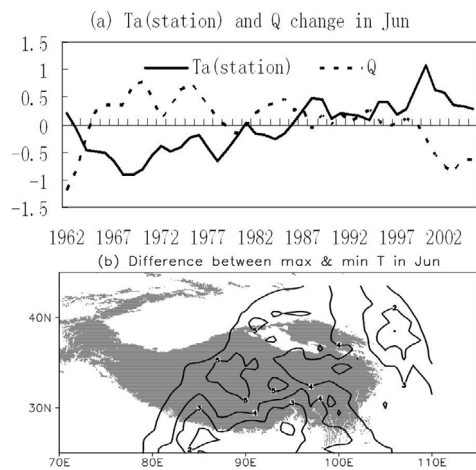


Figure 2. (a) The evolution of air temperature (T_a) at stations in the TP and heat source (Q) averaged in the region of ($27.5\text{--}37.5^\circ\text{N}$, $75\text{--}105^\circ\text{E}$) in June (units: K and W/m^2), and (b) the difference between year-to-year maximum and minimum of surface air temperature among the year of 1960–2005 (interval: 1 K). The time series for the indexes was normalized with dividing by the standard deviation and applied for a 5-year running mean. The shaded area shows the TP terrain.

[13] Figures 2a and 2b show the evolution of the five-year running mean TP surface air temperature averaged over the 90 Tibetan weather stations and the heat source averaged over ($27.5\text{--}37.5^\circ\text{N}$, $75\text{--}105^\circ\text{E}$) in June 1962–2005 and the difference between the year-to-year maximum and minimum of the surface air temperature during June 1960–2007 for each station (T_a difference), respectively. The difference may represent roughly the temperature trend through the examination of the temperature at the stations one by one. The majority of these weather stations were distributed in the eastern TP, as shown in Figure 1. The average air temperature continually rose about 2 K for 48 years, which is in agreement with calculation by Wang *et al.* [2008], whereas the heat source kept positive values during the majority of the period between the 1970s–1990s, but not for the periods of 1962–1964 and 1999–2005. The upstream airflow moving across the TP or some other mechanism may be why the column heat source did not respond to the surface heating clearly and instantly with the linear rising trend. The T_a difference showed a large region encompassed by the 5.0 K contour over the central TP, displaying a strong surface heating in the TP, as shown in Figure 2b. Previous studies have linked blocking occurring downstream from tropical convection via the propagation of equivalent barotropic Rossby wave propagation [e.g., Renwick and Revell, 1999]. However, studies about the linkage between the heating over high land in middle latitudes and blocking events were limited. Figure 3 shows the time series of an index measuring the intensity of a blocking high around the Okhotsk Sea in June (OKHI-1) during 1951–2000, which was adapted from Figure 2 of Wang and Lupo [2009]. Here, the unit of the index is the blocked day. The details about the OKHI-1 were addressed in Appendix B. The evolution of the OKHI-1 displayed an intermittent rising from the end

of 1950s to 2000, which suggests that the Okhotsk High is becoming more active gradually. The linear regression with the total increasing trend line indicated that the blocking days have significantly increased about four days in recent 50 years. The t-test showed significance at 99% confidence level for the trend. Since the development of the Okhotsk High accompanies the dispersion of the OKJ wave, the increase in frequency of the OKHI-1 implied that the OKJ propagation is occurring increasingly as well [Wang, 1992; Wang *et al.*, 2007]. Both the increasing trends of the OKHI-1 in Figure 3 and the air temperature over the TP in Figure 2a appeared roughly in the corresponding period.

[14] We cannot ignore the fact that the TP air temperature increased at a rate much faster than the global temperature, and this phenomenon may be closely related to global warming. The rapidly decreased TP snow cover, caused by global warming, can reduce the surface albedo over the TP. This will, in turn, accelerate TP warming as pointed out by many researchers [e.g., Yeh *et al.*, 1983]. Thus the decreased TP albedo can play a key role in enhancing the effect of the TP heat island. A detailed simulation for the reduced TP albedo will be addressed in section 4.

[15] Figures 4a, 4b show the correlation between Z500 and the TP air temperature and the TP heat source in June, respectively. Shaded areas indicate regions exceeding the 95% confidence level. The full arc line represented in the OKJ propagation track is picked up from the one marked with the letters A–F in Figure 3 of Wang *et al.* [2007]. Subjectively, the bold-dashed arc lines indicate the current wave train-like tracks. There is a possibility that two wave train-like patterns were located in the upstream and downstream regions of the TP, respectively, in Figure 4a. The upstream wave signal (i.e., from the Black Sea via Turkmenistan to the southeastern TP) appeared to be stronger than the downstream one (i.e., from the southeastern TP via the eastern border of Mongolia and the western Okhotsk Sea to the East Siberian Sea) although both of them lack statistical significance. It is difficult to say with certainty that there was a wave train following the OKJ track (full arc line) in Figure 4a. However, the downstream wave train-like pattern appears to show that a wave source over the TP was associated with positive or negative Z500 anomalies around the Okhotsk Sea, a result that coincides with the effect caused by the OKJ propagation. Note that the correlation in Figure 4a included an interaction between surface air temperature and Z500 with a positive feedback around the TP.

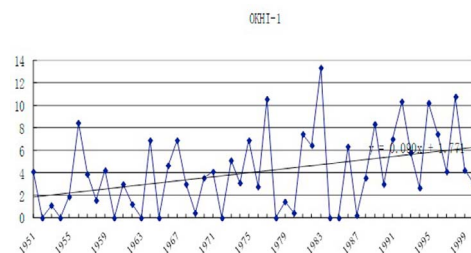


Figure 3. The evolution of the OKHI-1 in June (unit: blocked day). This was adapted from Figure 2 of Wang and Lupo [2009] with slight modification. The trend line (skew line) with the linear regression equation was plotted.

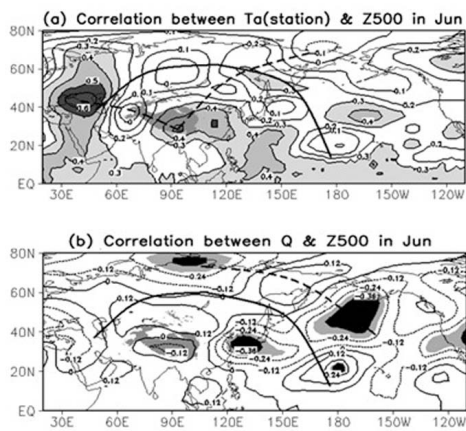


Figure 4. The correlation coefficient between Z500 and (a) Ta index and (b) Q index. All levels of the shaded regions indicate the confidence level exceeding 95%. The full arc line is the OKJ propagation track of previous studies and the bold-dashed arc lines indicate the current wave train-like tracks subjectively. The TP terrain is embedded by gray shade.

[16] The stronger wave train-like pattern is shown in Figure 4b. The correlation centers tilted northwest-southeast were located at 75°N, 95°E; 60°N, 150°E (near the Okhotsk Sea), and largely amplified at 50°N, 167.5°W, correspondingly. Although the values near the Okhotsk Sea were not significant, the correlations centered in the other two locations exceeded the 95% confidence level. The wave train track was close to the east part of the OKJ track (full arc line) and both patterns were nearly in the same phase in situ. Although there was no similar pattern occurring in Figure 4a, coincident with that in Figure 4b a significant positive correlation center was also found near the Okhotsk Sea.

[17] Lower values (below 2 m/s) of U500 were located around both the Okhotsk Sea and the TP and the higher one (over 8 m/s) was found between the two places as shown in Figure 5. This climatic distribution (the low-high-low zonal wind pattern) provides further evidence of the possibility of the wave train-like pattern as shown in Figure 4a. Note that the jet stream at 500 hPa over Asian continent was not strong compared with it at 200 hPa (the figure not shown), which may be one of the reasons why the OKJ wave does not propagate following the upper level jet stream (along

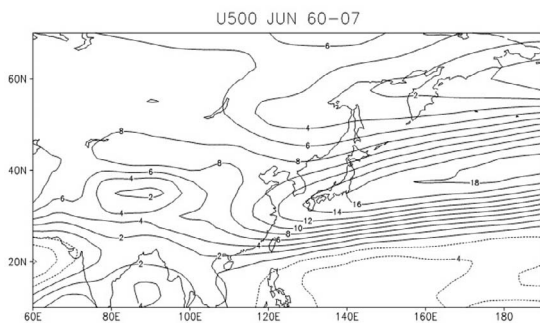


Figure 5. The distribution of the zonal wind at 500 hPa in June during 1960–2007 (interval: 2 m/s).

about 40°N latitude line) that acts as a waveguide as mentioned by Hoskins and Ambrizzi [1993]. Since the monthly mean was used in Figure 4, wave structure with smaller time scale tends to be hidden into the basic flow. The decorrelation time scale of the stationary Rossby wave in summer is generally less than one week [Wang et al., 2007]. The correlation analysis as an important procedure in checking wave train-like pattern is still needed for the monthly mean data. There is still a possibility that stationary Rossby waves become established along the dashed lines. The shape of the correlation centers suggested wave train-like structures that arranged along the dashed lines too. The phenomenon in Figures 4 and 5 implies that the Okhotsk High or the OKJ wave pattern tends to occur in response to a heating over the TP. Thus the TP might be another source region for the OKJ wave propagation in addition to that of the Caspian Sea. Note that there was another significant positive correlation center in Henan China (32.5°N, 110.25°E) except for the one in Southeast TP (Figure 4a). Additionally, there was no significant positive correlation area over the TP as shown in Figure 4b.

4. Effects of the TP Topography and Heating Using a Long Time Integration

[18] The CAM3.1 undertook the task of simulating climate variations over Eurasia by executing sensitivity experiments to determine the TP effects on long-time integration. Figures 6a, 6b, and 6c show the albedo, surface temperature, and the heat source of H-W run minus H-C run. The albedo anomalies below -0.24 were located over the central TP, indicating the effect of the artificial control of surface albedo in the model. Note that the albedo shown here has undergone a complex delivery process from CLM3.0 to CAM3.1. The long-time model integrations through various physical processes created lower values of the albedo than the originally imposed ones. Similarly, the positive surface

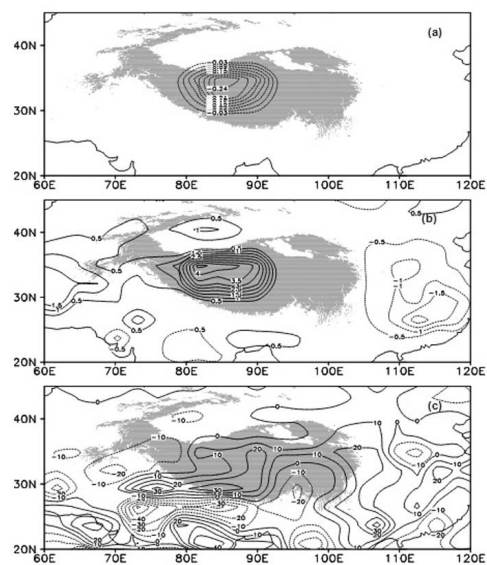


Figure 6. (a) The surface albedo (interval: 0.03), (b) the surface temperature (interval: 0.5 K) and (c) the heat source (interval: 10 W/m²) between the H-W run and H-C run.

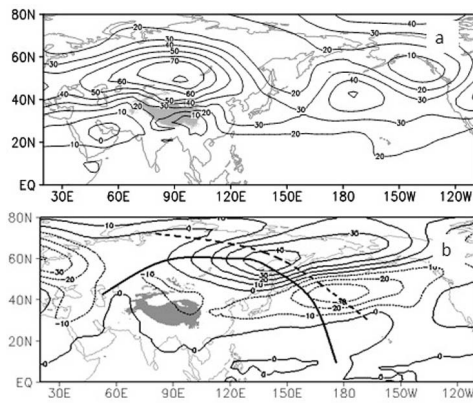


Figure 7. (a) The Z500 of UP-Ctr. run minus UP-ST run and (b) H-W run minus H-C run. The interval of the contour line is 10 gpm. The full line is the OKJ track and the bold-dashed line is the linkage of the wave train centers subjectively.

temperature anomaly over 4.5 K was centered over the TP, which was quantitatively and qualitatively analogous to the one in Figure 2b (*Since the surface temperature is close to the surface air temperature of TP, the surface temperature was chosen from CAM3.1 for the reason of brevity*). Further, the TP area was positively covered by the heat source anomaly with a center over 30 W/m^2 in the southwestern TP, as shown in Figure 6c. However, because the heat source was the integration from surface to the top of the troposphere, the maximum heat source was located in the southern TP not in central TP as the maximum surface temperature was shown. This bias is comprehensible. There was another large heat source center located over southern India, which was a remote effect due to the reduced TP albedo. The characteristics shown in Figure 6 ideally demonstrated a long-time AGCM integration due to the reduced albedo resulting from fast-melting snow cover on the TP, which was associated with global warming.

[19] Figures 7a, and 7b show the Z500 of the UP-Ctr. run minus the UP-ST run, and the Z500 of the H-W run minus H-C run in June, respectively. Note that the result in Figure 7a included the natural effects of the TP heating and the Himalayan torque resulting from the difference of the topography height between the two runs. The thermal effect with elevated topography could not be excluded and merged into the uplifting effect of the TP. A large positive anomaly (over 80 geopotential meter (gpm)) was centered at 50°N , 95°E , which is just north of the TP in Figure 7a. Since the only other high center near the International Date Line (IDL) in the North Pacific was weaker, no sign of the remote effect of the TP was found in the uplifting experiment. The difference between the two experiments would reflect greatly the thermal effects due to the elevation of the mountain, as well as the uplifting effects of the topography. In this season, such thermal effects might be rather significant. The sign in the high center to the north of the TP in Figure 7a coincides with the finding of the split flow in previous studies [e.g., Manabe and Terpstra, 1974]. Although Sato and Kimura [2007] pointed out that there were some seasonal changes of the airflow around the TP caused by the

mechanical forcing in their RegCM, the seasonal changes that involved a Rossby wave response was not obvious. Our experiments indicated that a positive height anomaly center north of the TP dominated in all seasons especially in winter, which resulted from the uplifting forcing of the TP (figures not shown). However, the wave train-like structure that appeared in Figure 7b was different; there was a positive anomaly center northwest of the Okhotsk Sea, a negative anomaly center at 47°N , 175°E and a positive anomaly center at 30°N , 165°W . The wave train-like pattern in Figure 7b was quite similar to the correlation result shown in Figure 4b, except for the slight drift of the low center near the IDL in the North Pacific. The wave-like track was closer than that in Figure 4b to the OKJ track. The charts for the experimental differences in other levels show similar patterns as those in Figure 7, which indicated the barotropic structure for the long time integration (figures omitted). Note that there was a weak height anomaly around the TP (-10 gpm) that coincided with the insignificant sign in situ in Figure 4b.

5. Effects of the TP Heating Using a Short Time Integration

[20] To investigate further the thermal effect of the TP, we used the RegCM3.1 to test the response of the atmospheric circulation to a heating source over the TP on the synoptic time scale. Here, the diabatic heating rate imposed in the RegCM3.1 was different from the change of the albedo as shown in section 4. The former was used to examine the sensitivity of the TP heating in a more rapidly varying process whereas the latter used a more slowly varying process. However, both heat sources were potentially associated with global climate warming. The method used for the change of the albedo shown in section 4 cannot represent the response of the circulation to the TP heating on the synoptic time scale. The slowly varying climate process is composed of many quickly varying synoptic processes. The diabatic heating rate added to the RegCM3.1 may represent just one member of many quickly varying processes. Although the simulations for the added diabatic heating rate from 2 K day^{-1} to 8 K day^{-1} on the TP were carried out, only the one for the 4 K day^{-1} heating rate is shown here for brevity.

[21] Figure 8 shows the geopotential height of H-Re4 run minus and ReB run at 850, 500, and 200 hPa on day 13, respectively. The positive and negative height anomaly centers were systematically arranged from the TP via the Okhotsk Sea to the sea area east of Japan, presenting a clear Rossby wave train, especially at 200 hPa on day 13. The positions of the negative center below -250 gpm at 50°N , 122.5°E , the positive one over 100 gpm in the Okhotsk Sea, and the negative one below -50 gpm east of Japan Island at 500 hPa coincided with the correlation centers marked with C, D, and E in Figure 3 of Wang *et al.* [2007]. Thus the Rossby wave excited by the heating over the TP is in agreement with the positive phase of the eastern OKJ pattern. Note that the dashed line in Figure 8b was quite close to that in the downstream area of the TP (Figure 4a). This implies that the wave train response to the warm surface over the TP as shown in Figure 4a is quite plausible in spite

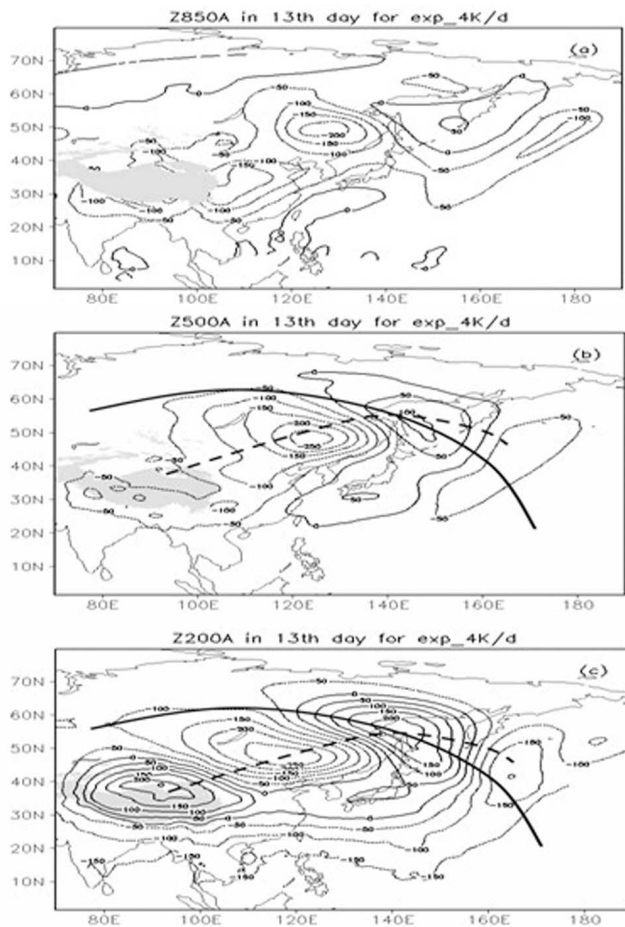


Figure 8. The geopotential height of H-Re4 run minus ReB run at (a) 850, (b) 500, and (c) 200 hPa. The contour line interval is 50 gpm. The full line shows the OKJ track and the bold-dashed line is the linkage of the wave train centers subjectively.

of the lack of statistical significance in the correlation center to the northeast of the TP.

[22] Figure 9 shows the geopotential height at 200 hPa and the surface temperature of H-Re4 run minus ReB run on the odd days; i.e., days 1, 3, 5, 7, 9, and 11 respectively. For brevity, we did not show the figures on the even days or after day 13. There were three stages representing the wave train formation. A change of the circulation started during the first three days when a positive height anomaly was generated from a negative one in the TP; i.e., the wave source region. Then, positive and negative height anomaly centers alternately spread roughly along the dashed track during days 4–8 when a wave train-like structure appeared. Last, the phase of the wave train was approximately fixed during days 9–15. The phase of the wave train largely shifted downstream and the wave train collapsed finally after day 16 due to the expanding of the errors of lateral boundary and its limited decorrelation time scale. The positive surface temperature anomaly showed a robust center of about 4–7 K in the TP and rapidly spread to surrounding areas at about 2–3 K in the first two days. This large center, strengthening to about 8–10 K, dominated in

the most of the following simulated days. The temperature wave train-like structure corresponding with the height wave train appeared during days 9–15.

[23] A similar phenomenon was found in other experiments, i.e., the height of the sensitivity experiments of H-Re2, H-Re6, and H-Re8 runs minus the model climatological mean. Figures 10 and 11 show the anomalies of Z500 and Z200 picked up along the dashed track in Figure 8 on day 5 and day 10 with the diabatic heating rates from 2 K to 8 K in the model experiments, respectively. Note that the dashed track in Figure 8 may not link with the anomaly centers for other days of all the experiments. Yet, the amplitudes of the anomalies near the center positions in Figure 8 tended to be larger with the imposed higher diabatic heating rates as shown in Figures 10 and 11. The atmospheric response to the forced heating on the TP was found to be sensitive, although we were not able to give related figures for all of the experiments. By comparing all four of our experiments against different diabatic heating rates, we found that the stronger the heating over the TP became in our model, the faster and stronger was the Rossby wave produced. The circulations appear to be responding linearly to the different heating rates. The path of the propagating anomaly centers can be recognized as the “great circle” proposed by *Hoskins and Karoly* [1981], which roughly matched a stationary Rossby wave with the zonal wave number 5, as similarly calculated by *Wang et al.* [2007]. The three-dimensional images from 850–200 hPa displayed an equivalent barotropic structure for the generated Rossby wave, except for that within the wave source region near the TP, as shown in Figure 8. The baroclinic structure near the wave source over the TP shows a character similar to that in the tropics.

6. Discussion and Summary

[24] The climatic simulations roughly coincided with the diagnostic analysis, although there were some differences between them. The high surface temperature of the TP in association with global climate warming was produced successfully by the AGCM simulation comparing Figure 2b to Figure 6b. Both figures showed a high temperature center of about 4.5–6 K located in central TP. However, the TP surface warming does not mean that there was warming in the whole troposphere over the TP, as shown in the two observational curves in Figure 2a. The simulated increase of the column heat source in Figure 6c displayed an ideal heating process: a heating diffusion to upper-level air from the surface warming due to the reduced surface albedo. The simulation is still relevant to the real atmosphere because the local surface warming is mainly diffused into the high-level air over the TP with the increasing progression of global warming; the reduced surface albedo will play a crucial role in heating the atmosphere over the TP. No matter what the reason for the large differences between the correlation results about surface warming (Figure 4a) and the warming in whole troposphere over the TP (Figure 4b), all of TP warmings were associated with a significant positive Z500 anomaly around the Okhotsk Sea. This coincided with the impact of the OKJ propagation in a positive phase. This implies that the simulation result; i.e., the wave propagation generated by TP warming, could contribute to a positive

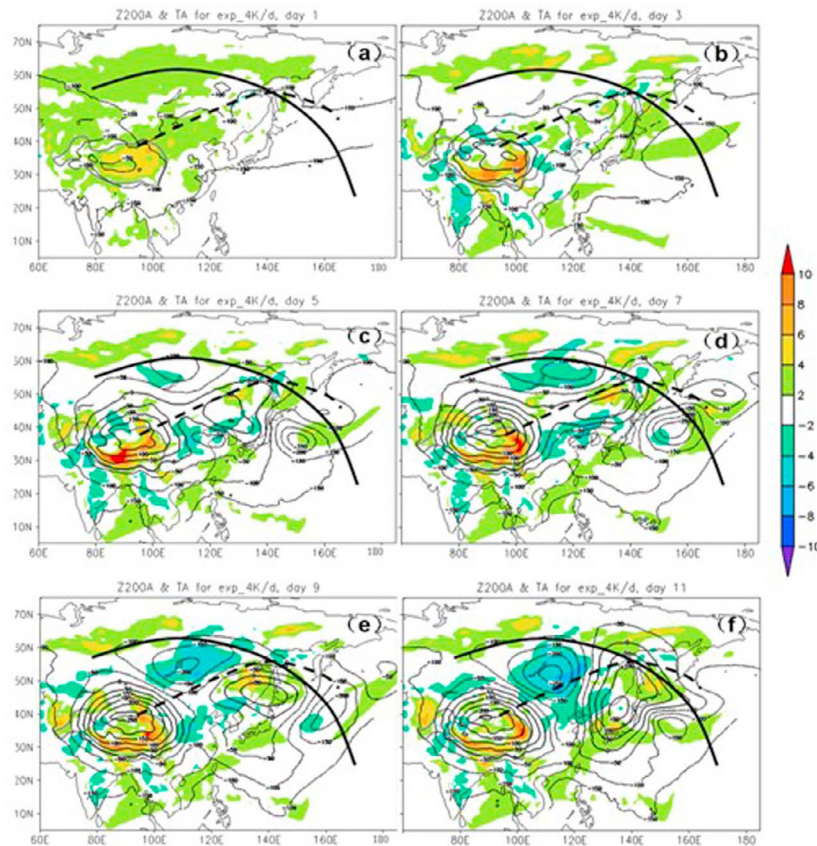


Figure 9. The geopotential height at 200 hPa (contour lines with an interval of 50 gpm) and the surface temperature (color images with the interval of 2 K) of H–Re4 run minus ReB run on day 1, 3, 5, 7, 9, and 11, respectively. The full line and the bold dashed line were picked up from Figure 8c.

Z500 anomaly around the Okhotsk Sea, as shown in Figures 7b and 8 and roughly supported by the observations. The downstream wave train-like track in Figure 4a (Figure 4b) is close to that shown in Figure 8 (Figure 7b). This suggests that the wave train-like structure tends to be traced back to the TP where it was generated by a direct surface heating over the TP. However, the tracing could not be found when the deep heating occurred in the troposphere over the TP (Figure 4b) or the surface heating was added into the CAM3.1 by changing albedo through a complex physical process in long time model integration (Figure 7b). The heating added in a more gradual manner resulted in the generation of a more stationary and more permanent wave train pattern away from the TP, in which the local response of the circulation to the original deep heating over the TP evolves over a longer period of time. This wave train pattern downstream from the TP behaves as an internal atmospheric oscillation that was initiated by a deep heating over the TP. Gaining a better understanding of the mechanism for the formation of the wave train pattern, however, will require further study using more AGCM simulations.

[25] We found one of the strongest pieces of evidence for the propagation of a Rossby wave to be the equivalent barotropic structure of a wave train that appeared in every resulting simulation and observational analysis of the impact of TP warming. However, the height anomalies near the TP appeared to be baroclinic, as shown in Figures 8a–8c, which

resulted from the surface heating and an exponential damping of this heating with increasing height in the troposphere over the TP. The surface heating served as the Rossby wave source similar to that near the tropics. The convective upward airflow was quite strong over the TP as well (figures omitted). In spite of this, and unlike in the tropics, a barotropic high with a warm core or a low with a cold core tends to appear in higher latitudes, so the baroclinic structure near the TP did not appear in the long time integration as shown in Figure 7b. Compared with Figure 7b, the wave train structure in Figure 8 provided further evidence of the remote thermal effects of the TP on the atmosphere.

[26] Wave train-like correlation centers linked by a boldface dashed line in Figure 4a lined up from upstream regions of Black Sea to the TP. This implies that Rossby wave propagation upstream may cool or heat air over the TP directly in spite of the wave pattern being weak. Upstream Rossby wave propagation that could change the warming rate for the air temperature over the TP might be one reason why the surface warming did not coincide with the column warming over the TP, as shown in Figure 2a.

[27] Although the AGCM simulation for the altered albedo environment was adopted in a similar manner to that of Wang *et al.* [2008], the end result was different, as can be seen by comparing Figure 7b in this paper to Figure 2b in that paper. The difference may be considered from two points: (1) They examined objects through a whole summer

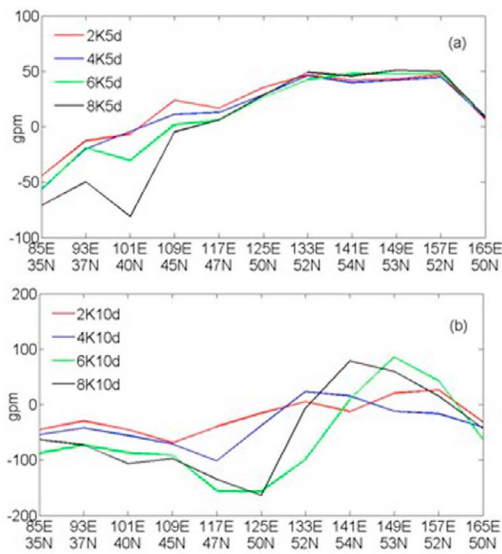


Figure 10. The anomalies of Z500 picked up along the dashed track in Figure 8 on (a) day 5 and (b) day 10 with the diabatic heating rates from 2–8 K in the model experiments, respectively. The unit is gpm.

(June, July, and August) while we focused only on the month of June; and (2) we used a different AGCM. Wang [1992] pointed out that each summer month has its own circulation pattern in Eurasia due to the seasonal progress. In particular, the period of the Meiyu/Baiu subsystem of the summer monsoon dominates over East Asia in the month of June and thus produces a circulation pattern with characteristics distinct from the other summer months of July and August. This explains why the atmospheric circulation response to the TP thermal source is different when considering June only, rather than the whole summer. A positive height anomaly around the Okhotsk Sea in response to the TP heating implied that the TP can affect Meiyu/Baiu system indirectly since the Okhotsk high plays roles in keeping Meiyu front more steadily and shifting the Baiu front farther southward [Wang, 1992]. In our opinion, the circulation changes in July and August might be much more complex than that in June because the stationary systems such as Meiyu/Baiu or blocking high over Northeast Asia would disappear in late summer. The study especially for July and August is expected in future. On the other hand, the CAM3.1, as adopted for this study, was armed with more comprehensive physical processes, including a connection with the CLM3.0. A rising temperature about 4.5 K was created by reducing and increasing surface albedo by only about 0.05 in the model, which was closer to what was found by direct observation. To understand the differences between the two AGCMs would require further simulations of the response of atmospheric circulation to TP warming.

[28] The IPCC [2007] concluded that most of the observed temperature increases since the middle of the 20th century were very likely caused by increasing concentrations of greenhouse gases resulting from human activity such as fossil fuel burning and deforestation. This climate warming is strongly associated with the continuing retreat of glaciers, the permafrost, and sea ice, which causes the

reduction of the in situ surface albedo. Such impacts of global warming quickened the pace of TP warming. Although the correlation between the time series of the OKHI-1 and the TP surface air temperature was poor as shown in section 3, the coincidence of both trends rising indicated that they had similar decadal variation. This relationship might suggest that TP warming accelerated by global climate warming increased the frequency of the OKJ propagation in the east because the Okhotsk High tends to be associated with an in situ Rossby wave dispersion, as mentioned in section 3.

[29] We concluded that because the wave path from the TP via the Okhotsk Sea to the downstream area lies largely to the north of the climatic position of the westerly jet stream (along the latitude line of about 40°N), the Rossby wave propagation excited by the TP thermal forcing does not follow the waveguide theory proposed by Hoskins and Ambrizzi [1993]. This implies that the westerly jet stream in June is not strong enough to trap the Rossby wave generated by a robust TP heating source. In fact, the subtropical westerly jet over the Asian continent in June is weaker than that over the Western Pacific, which might suggest that the jet has less power to control the propagation of the OKJ-like wave. The unique topography and strong air-sea temperature contrast around the Okhotsk Sea create a favorable environment for forming the eastern part of the OKJ propagation [Wang et al., 2007].

[30] In summary, the uplifting effect of the TP, including air made warmer by the huge topography than its surroundings climatologically, results mainly in a local response in the atmosphere; i.e., a large ridge north of the TP in the troposphere in June. There was no Rossby wave response to the uplifting effect. However, the anomalous TP atmospheric heating associated with global warming tends to excite a Rossby wave originating from the TP via the Lake Baikal region and continuing to move through the Okhotsk Sea to downstream areas. The appearance of the Rossby wave coincides with the positive phase of the eastern part of the OKJ propagation. Thus the TP atmospheric heating acts

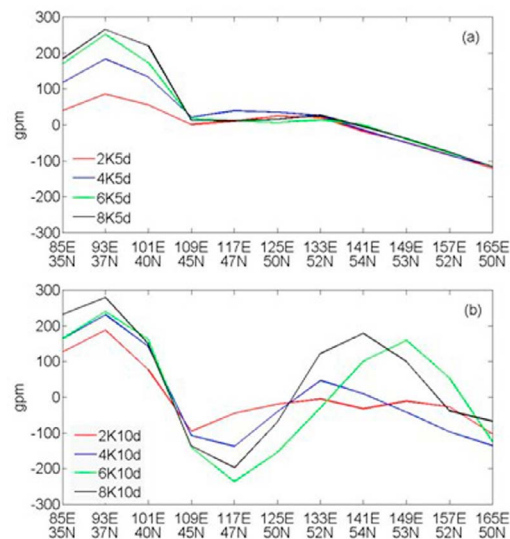


Figure 11. Same as Figure 10 except for the anomalies of Z200.

as an additional wave source in relaying and enhancing the eastern part of the OKJ wave propagation. Its path usually lies beyond the latitude line of 40°N, which is where the westerly jet stream takes over the role of waveguide.

Appendix A

[31] Based on the method provided by Yanai *et al.* [1992], the diabatic heat source was calculated by using

$$Q = SH + LH + RC \quad (A1)$$

where SH , LH , and RC are the surface sensible heat flux, latent heat flux by precipitation, and radiation net flux, respectively. Then Q was vertically integrated from surface to the top of the troposphere in this study and

$$LH = L_w \times Pr \quad (A2)$$

where $L_w = 2.5 \times 10^6 \text{ J kg}^{-1}$ is the coefficient for latent heat flux (vaporization). Pr is the precipitable rate with a unit of $\text{kg m}^{-2} \text{ s}^{-1}$.

$$RC = LR_1 - LR_2 + SR \quad (A3)$$

here LR_1 , LR_2 , and SR are the surface long wave radiation net flux, outgoing longwave radiation at the tropopause and the absorption of solar radiation by the air column of a unit cross-section area, respectively. SR is the function of the surface net longwave radiation flux, downward/upward solar radiation flux at the tropopause.

Appendix B

[32] The blocking high is described here by using the blocking index of Tibaldi and Molteni [1990], who stated that the blocking index is a coarse-resolution local maximum of the 5 day averaged 500 hPa height on a given meridian. The formula is as follows:

$$\begin{aligned} GHG1(\lambda, t) &= \frac{z(\phi_0, \lambda, t) - z(\phi_-, \lambda, t)}{\phi_0 - \phi_-} \\ GHG2(\lambda, t) &= \frac{z(\phi_+, \lambda, t) - z(\phi_0, \lambda, t)}{\phi_+ - \phi_0} \end{aligned} \quad (B1)$$

where z is the 5 day running mean of geopotential height at 500 hPa,

$$\begin{aligned} \phi_0 &= 60^\circ\text{N} + \Delta \\ \phi_+ &= \phi_0 + 20^\circ + \Delta \\ \phi_- &= \phi_0 - 20^\circ + \Delta \end{aligned} \quad (B2)$$

and

$$\Delta = -5^\circ, 0^\circ, \text{ or } +5^\circ \quad (B3)$$

The circulation is judged to be blocked at longitude λ and time t and only if;

$$GHG1(\lambda, t) > 0 \text{ and } GHG2(\lambda, t) < -10 \text{ m deg}^{-1} \quad (B4)$$

for at least one value of Δ in (B3).

[33] OKHI-1 for the Okhotsk High was calculated by averaging the blocking days from 130°E to 150°E.

[34] **Acknowledgments.** We thank the editors and the two anonymous reviewers for their valuable suggestions and comments. The first author appreciates Ms. Mary Golden, the ESL coach for her helpful advice and kind encouragement. This work was jointly supported by the JICA project of China-Japan Center of the Cooperative Research on Meteorological Disaster, the International Sci-Tech Cooperative Project (2009DFB20540), the special scientific research project of China commonwealth trade (meteorology) (GYHY201006009).

References

- Collins, W. D., et al. (2004) Description of the NCAR Community Atmosphere Model (CAM 3.0), *Tech. Rep. NCAR/TN-464+STR*, 210 pp., Natl. Cent. for Atmos. Res., Boulder, Colo.
- Hahn, D. G., and S. Manabe (1975), The role of mountains in the South Asian monsoon circulation, *J. Atmos. Sci.*, *32*, 1515–1541, doi:10.1175/1520-0469(1975)032<1515:TROMIT>2.0.CO;2.
- Hoskins, B. J., and T. Ambrizzi (1993), Rossby wave propagation on a realistic longitudinally varying flow, *J. Atmos. Sci.*, *50*, 1661–1671, doi:10.1175/1520-0469(1993)050<1661:RWPOAR>2.0.CO;2.
- Hoskins, B. J., and D. J. Karoly (1981), The steady linear response of a spherical atmosphere to thermal and orographic forcing, *J. Atmos. Sci.*, *38*, 1179–1196, doi:10.1175/1520-0469(1981)038<1179:TSLR0A>2.0.CO;2.
- Intergovernmental Panel on Climate Change (IPCC) (2007), Summary for policymakers, in *Climate Change 2007: The Physical Science Basis: Working Group I Contribution to the Fourth Assessment Report of the IPCC*, edited by S. Solomon et al., pp. 1–18, Cambridge Univ. Press, New York. [Available at <http://www.ipcc.ch/pdf/assessment-report/ar4/wg1/ar4-wg1-spm.pdf>]
- Iskenderian, H., and D. A. Salstein (1998), Regional sources of mountain torque variability and high-frequency fluctuations in atmospheric angular momentum, *Mon. Weather Rev.*, *126*, 1681–1694, doi:10.1175/1520-0493(1998)126<1681:RSOMTV>2.0.CO;2.
- Kalnay, E., et al. (1996), The NCEP/NCAR 40-year reanalysis project, *Bull. Am. Meteorol. Soc.*, *77*, 437–471, doi:10.1175/1520-0477(1996)077<0437:TNYRYP>2.0.CO;2.
- Kato, K. (1989), Seasonal transition of the lower-level circulation systems around the Baiu front in China in 1979 and its relation to the northern summer monsoon, *J. Meteorol. Soc. Jpn.*, *67*, 249–265.
- Liu, Y., B. Hoskins, and M. Blackburn (2007), Impact of Tibetan orography and heating on the summer flow over Asia, *J. Meteorol. Soc. Jpn.*, *85B*, 1–19, doi:10.2151/jmsj.85B.1.
- Lott, F., A. W. Robertson, and M. Ghil (2001), Mountain torques and atmospheric oscillations, *Geophys. Res. Lett.*, *28*, 1207–1210, doi:10.1029/2000GL011829.
- Manabe, S., and T. B. Terpstra (1974), The effects of mountain on the general circulation of the atmosphere as identified by numerical experiments, *J. Atmos. Sci.*, *31*, 3–42, doi:10.1175/1520-0469(1974)031<0003:TEOMOT>2.0.CO;2.
- Murakami, T. (1981), Orographic influence of the Tibetan Plateau on the Asiatic winter monsoon circulation Part I: Large-scale aspects, *J. Meteorol. Soc. Jpn.*, *59*, 40–65.
- Nakamura, H., and T. Fukamachi (2004), Evolution and dynamics of summertime blocking over the Far East and the associated surface Okhotsk High, *Q. J. R. Meteorol. Soc.*, *130*, 1213–1233, doi:10.1256/qj.03.101.
- Ogi, M., Y. Tachibana, and K. Yamazaki (2004), The connectivity of the winter North Atlantic Oscillation (NAO) and the summer Okhotsk High, *J. Meteorol. Soc. Jpn.*, *82*, 905–913, doi:10.2151/jmsj.2004.905.
- Rayner, N. A., D. E. Parker, E. B. Horton, C. K. Folland, L. V. Alexander, D. P. Powell, E. C. Kent, and A. Kaplan (2003), Global analyses of sea surface temperature, sea ice, and night marine air temperature since the late nineteenth century, *J. Geophys. Res.*, *108*(D14), 4407, doi:10.1029/2002JD002670.
- Renwick, J. A., and M. J. Revell (1999), Blocking over the South Pacific and Rossby wave propagation, *Mon. Weather Rev.*, *127*, 2233–2247, doi:10.1175/1520-0493(1999)127<2233:BOTSPA>2.0.CO;2.
- Reynolds, R., N. Rayner, T. Smith, D. Stokes, and W. Wang (2002), An improved in situ and satellite SST analysis for climate, *J. Clim.*, *15*, 1609–1625, doi:10.1175/1520-0442(2002)015<1609:AIHSAS>2.0.CO;2.
- Sato, N., and M. Takahashi (2006), Dynamical processes related to the appearance of quasi-stationary waves on the subtropical jet in the mid-summer Northern Hemisphere, *J. Clim.*, *19*(8), 1531–1544, doi:10.1175/JCLI3697.1.

- Sato, N., and M. Takahashi (2007), Dynamical processes related to the appearance of the Okhotsk high during early midsummer, *J. Clim.*, *20*, 4982–4994, doi:10.1175/JCLI4285.1.
- Sato, T., and F. Kimura (2007), How does the Tibetan Plateau affect the transition of Indian monsoon rainfall?, *Mon. Weather Rev.*, *135*, 2006–2015, doi:10.1175/MWR3386.1.
- Tibaldi, S., and F. Molteni (1990), On the operational predictability of blocking, *Tellus, Ser. A*, *42*, 343–365, doi:10.1034/j.1600-0870.1990.t01-2-00003.x.
- Tilly, D. E., A. R. Lupo, C. J. Melick, and P. S. Market (2008), Calculated height tendencies in a Southern Hemisphere blocking and cyclone event: The contribution of diabatic heating to block intensification, *Mon. Weather Rev.*, *136*, 3568–3578, doi:10.1175/2008MWR2374.1.
- Wang, B., Q. Bao, B. Hoskins, G. Wu, and Y. Liu (2008), Tibetan Plateau warming and precipitation changes in East Asia, *Geophys. Res. Lett.*, *35*, L14702, doi:10.1029/2008GL034330.
- Wang, Y. (1992), Effects of blocking anticyclones in Eurasia in the rainy season (Meiyu/Baiu season), *J. Meteorol. Soc. Jpn.*, *70*, 929–951.
- Wang, Y., and A. R. Lupo (2009), An extratropical air-sea interaction over the North Pacific in association with a preceding El Niño episode in early summer, *Mon. Weather Rev.*, *137*, 3771–3785, doi:10.1175/2009MWR2949.1.
- Wang, Y., and T. Yasunari (1994), A diagnostic analysis of the wave train propagating from high-latitudes to low-latitudes in early summer, *J. Meteorol. Soc. Jpn.*, *72*, 269–279.
- Wang, Y., K. Yamazaki, and Y. Fujiyoshi (2007), The interaction between two separate propagations of Rossby waves, *Mon. Weather Rev.*, *135*, 3521–3540, doi:10.1175/MWR3486.1.
- Weickmann, K. M. (2003), Mountains, the global frictional torque, and the circulation over the Pacific–North American region, *Mon. Weather Rev.*, *131*, 2608–2622, doi:10.1175/1520-0493(2003)131<2608:MTGFTA>2.0.CO;2.
- Yanai, M., C. Li, and Z. Song (1992), Seasonal heating of the Tibetan Plateau and its effects on the evolution of the Asian summer monsoon, *J. Meteorol. Soc. Jpn.*, *70*, 319–351.
- Ye, T. C., and G. Wu (1998), The role of the heat source of the Tibetan Plateau in the general circulation, *Meteorol. Atmos. Phys.*, *67*, 181–198, doi:10.1007/BF01277509.
- Yeh, T. C., R. Wetherald, and S. Manabe (1983), A model study of the short-term climatic and hydrologic effects of sudden snow-cover removal, *Mon. Weather Rev.*, *111*, 1013–1024, doi:10.1175/1520-0493(1983)111<1013:AMSOTS>2.0.CO;2.

P. Li, Shanxi Meteorological Bureau, Shanxi Meteorological Observatory, No.36 Beiguanzhengjie, Xian, Shaanxi 710014, China.

A. R. Lupo, Department of Soil, Environment and Atmospheric Sciences, University of Missouri, Columbia, MO 65211, USA.

Y. Wang and X. Xu, State Key Laboratory of Severe Weather, Chinese Academy of Meteorological Sciences, 46 Zhongguancun Southern Street, Haidian, Beijing 100081, China. (yfwang@cma.gov.cn)

Z. Yin, Beijing Meteorological Bureau, Beijing 100097, China.